



---

## Transient Analysis of Heat and Mass Transfer by Natural Convection in Power-Law Fluid past a Vertical Plate Immersed in a Porous Medium (Numerical Study)

**Nasser S. Elgazery**

Preparatory Year Unit  
Al-Qassim University  
P.O. Box 6595

Al-Qassim, Buraidah, 51452 Saudi Arabia

Received: April 22, 2008; Accepted: November 9, 2008

### Abstract

This paper attempted a numerical examination of the problem of unsteady free convection with heat and mass transfer from an isothermal vertical flat plate to a non-newtonian fluid saturated porous medium. The flow in the porous medium was described via the Darcy-Brinkman-Forchheimer model. The simultaneous development of the problem of boundary layers was obtained numerically by finite difference method. Boundary layer and Boussinesq approximations had been incorporated. Numerical calculations were carried out for the various parameters entering into the problem. Velocity, temperature and concentration profiles were shown graphically and the physical quantities of the problem were given in tables. It was found that as time approaches infinity, the values of friction factor, heat transfer and mass transfer coefficients approach the steady state values.

**Key words:** Finite Difference Method, Non-Newtonian Power-law Fluids, Non-Darcy Porous Medium, Heat and Mass Transfers, Natural Convection

**AMS 2000 Subject Classification Numbers:** 65N06, 76S05, 76D05

### 1. Introduction

A number of industrially important fluids such as foods, polymers, molten plastics, slurries and pulps display non-Newtonian fluid behavior. Non-Newtonian fluids exhibit a non-linear relationship between shear stress and shear rate. Its worth mentioning here that many of the inelastic non-Newtonian fluids encountered in chemical engineering processes, are known to

follow the empirical Ostwald-de-Waele model or the so-called “power-law model” in which the shear stress varies according to a power function of the strain rate.

The convection heat and mass transfer from surface embedded in Non-Newtonian fluids find several applications in geothermal engineering, petroleum recovery, filtration processes, oil extraction, solid matrix heat exchangers, thermal insulation, storage of nuclear waste materials, packed beds, porous insulation, beds of fossil fuels, nuclear waste disposal, resin transfer modeling, etc. Also, it is worth mentioning that non-Darcian forced flow boundary layers form a very important group of flows, the solution of which is of great importance in many practical applications such as in biomechanical problems, in filtration transpiration cooling and geothermal. Pascal (1992) presented similarity solutions for axisymmetric plane radial power law fluid flows through a porous medium. Darcy-Forchheimer natural, forced and mixed convection heat transfer in power-law fluid saturated porous media was studied by Shenoy (1993).

The problem of forced convection heat transfer on a flat plate embedded in porous media for power-law fluids has been studied by Hady and Ibrahim (1997). Kinyanjui, et al. (2001) studied the magnetohydrodynamic free convection heat and mass transfer of a heat generating fluid past an impulsively started infinite vertical porous plate with Hall current and radiation absorption. Anwar Hossain and Wilson (2002) discussed the Natural convection flow in a fluid-saturated porous medium enclosed by non-isothermal walls with heat generation. Numerical modeling of non-Newtonian fluid flow in a porous medium using a three dimensional periodic array was presented by Inoue and Nakayama (1998).

All these studies were concerned with steady flows. Pascal (1992) presented similarity solutions to some unsteady flows of non-Newtonian fluids of power law behavior. Pascal and Pascal (1997) studied the non-linear effects on some unsteady non-Darcian flows through porous media. Unsteady forced convection heat transfer on a flat plate embedded in the fluid-saturated porous medium with inertia effect and thermal dispersion is investigated by Wen and Hsiao (2002). Israel-Cookey et al. (2003) discussed the influence of viscous dissipation and radiation on unsteady MHD free-convection flow past an infinite heated vertical plate in a porous medium with time-dependent suction. Recently, Kok Siong Chiem and Yong Zhao (2004) studied the problem of numerical study of steady/unsteady flow and heat transfer in porous media using a characteristics-based matrix-free implicit FV method on unstructured grids.

The purpose of this paper is to study the problem of unsteady free convection with heat and mass transfer from an isothermal vertical flat plate to a non-Newtonian power-law fluid saturated porous medium. The Darcy-Brinkman-Forchheimer model which includes the effects of boundary and inertia forces was employed. The dimensionless non-linear partial differential equations were solved numerically using an explicit finite-difference scheme. The values of friction factor and heat transfer coefficient were determined for steady and unsteady free convection.

## 2. Mathematical formulation

Consider the unsteady, laminar boundary layer in a two-dimensional natural convective flow of a non-Newtonian fluid over a vertical flat plate embedded in a porous medium with heat and mass transfer (see Figure 1). At time  $\bar{t} = 0$ , the temperature of the surface immersed in a fluid is raised suddenly from that of surrounding fluid  $\bar{T}_\infty$ , up to a higher and constant value  $\bar{T}_w$  and kept at this value thereafter. Also,  $\bar{C}_\infty$  is the species concentration in the fluid far away from the plate and  $\bar{C}_w$  the species concentration at the plate. Under the Boussinesq and boundary layer approximations, the governing mass, momentum, concentration and energy conservation equations become:

$$\frac{\partial \bar{u}}{\partial \bar{x}} + \frac{\partial \bar{v}}{\partial \bar{y}} = 0 \quad (1)$$

$$\rho \left( \frac{\partial \bar{u}}{\partial \bar{t}} + \bar{u} \frac{\partial \bar{u}}{\partial \bar{x}} + \bar{v} \frac{\partial \bar{u}}{\partial \bar{y}} \right) = \nabla P,$$

where

$$\frac{1}{k} (-\nabla P + \bar{\rho}g) = -\frac{\partial}{\partial \bar{y}} \left( \left| \frac{\partial \bar{u}}{\partial \bar{y}} \right|^{n-1} \frac{\partial \bar{u}}{\partial \bar{y}} \right) + \frac{\varepsilon^n}{K} |\bar{u}|^{n-1} \bar{u} + \frac{\rho F \varepsilon^2}{k K^{1/2}} |\bar{u}| \bar{u},$$

and

$$\bar{\rho} = \rho [\beta(\bar{T} - \bar{T}_\infty) + \beta^*(\bar{C} - \bar{C}_\infty)].$$

Then,

$$\begin{aligned} \frac{\partial \bar{u}}{\partial \bar{t}} + \bar{u} \frac{\partial \bar{u}}{\partial \bar{x}} + \bar{v} \frac{\partial \bar{u}}{\partial \bar{y}} &= g\beta(\bar{T} - \bar{T}_\infty) + g\beta^*(\bar{C} - \bar{C}_\infty) \\ &+ \frac{k}{\rho} \frac{\partial}{\partial \bar{y}} \left( \left| \frac{\partial \bar{u}}{\partial \bar{y}} \right|^{n-1} \frac{\partial \bar{u}}{\partial \bar{y}} \right) - \frac{k\varepsilon^n}{\rho K} |\bar{u}|^{n-1} \bar{u} - \frac{F\varepsilon^2}{K^{1/2}} |\bar{u}| \bar{u} \end{aligned} \quad (2)$$

$$\frac{\partial \bar{T}}{\partial \bar{t}} + \bar{u} \frac{\partial \bar{T}}{\partial \bar{x}} + \bar{v} \frac{\partial \bar{T}}{\partial \bar{y}} = \frac{k_f}{\rho c_p} \frac{\partial^2 \bar{T}}{\partial \bar{y}^2} + \frac{D_m k_T}{c_s c_p} \frac{\partial^2 \bar{C}}{\partial \bar{y}^2} \quad (3)$$

$$\frac{\partial \bar{C}}{\partial \bar{t}} + \bar{u} \frac{\partial \bar{C}}{\partial \bar{x}} + \bar{v} \frac{\partial \bar{C}}{\partial \bar{y}} = D_m \frac{\partial^2 \bar{C}}{\partial \bar{y}^2} + \frac{D_m k_T}{T_m} \frac{\partial^2 \bar{T}}{\partial \bar{y}^2} \quad (4)$$

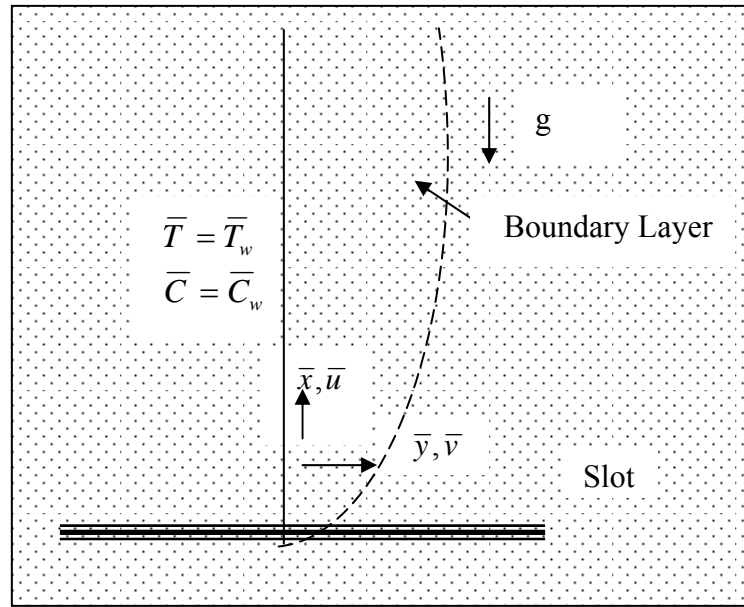


Figure 1. Coordinate system for the physical model of the problem.

In the previous equations,  $(\bar{u}, \bar{v})$  are the velocity components along  $\bar{x}$  and  $\bar{y}$  axis. The temperature of the surface is  $\bar{T}_w$  and far away from the surface this value is invariant and is represented by  $\bar{T}_\infty$ . Also, the concentration of the surface is  $\bar{C}_w$  and far away from the surface this value is invariant and is represented by  $\bar{C}_\infty$ .  $P$  is the pressure.  $\rho, \beta, \beta^*$  are the density, the volumetric coefficient of thermal expansion and the coefficient of expansion with concentration, respectively.  $\varepsilon, F, K$  are the porosity, the empirical constant and the permeability, respectively.  $k, k_f, c_p, g$  are the non-Newtonian consistency index, the fluid thermal conductivity, the fluid specific heat and the acceleration due to gravity, respectively.  $c_s, k_T, D_m, T_m$  are the concentration susceptibility, the fluid thermal diffusion ratio, the coefficient at mass diffusivity and the mean fluid temperature, respectively.

The initial and boundary conditions are:

$$\begin{aligned} \bar{t} = 0: & \quad \bar{u} = \bar{v} = 0, \bar{T} = \bar{T}_\infty, \bar{C} = \bar{C}_\infty \quad \text{for all } \bar{x} \text{ and } \bar{y} \\ \bar{t} > 0: & \quad \begin{cases} \bar{u} = \bar{v} = 0, \bar{T} = \bar{T}_\infty, \bar{C} = \bar{C}_\infty & \text{at } \bar{x} = 0, \forall \bar{y} \\ \bar{u} = \bar{v} = 0, \bar{T} = \bar{T}_w, \bar{C} = \bar{C}_w & \text{at } \bar{x} > 0, \bar{y} = 0 \\ \bar{u} = 0, \bar{T} \rightarrow \bar{T}_\infty, \bar{C} \rightarrow \bar{C}_\infty & \text{at } \bar{x} > 0 \text{ as } \bar{y} \rightarrow \infty \end{cases} \end{aligned} \quad (5)$$

In this study, in accordance with previous work reported by Shulman et al. (1975) and Shvets and Vishnevskiy (1987) the following transport properties based on the power-law model are assumed to hold

$$\tau_{ij} = -p\delta_{ij} + k \left| \frac{1}{2} I_2 \right|^{(n-1)/2} e_{ij}, \tag{6a}$$

where  $\tau_{ij}$  and  $e_{ij}$  are the tensors of stress and strain rate,  $\delta_{ij}$  is the unit tensor,  $I_2$  is the second invariant of the strain rate,  $p$  is the pressure and  $n$  is the power flow behavior index of the fluid ( $n > 0$ ). For  $n = 1$ , it reduces to a Newtonian fluid, for values of  $n < 1$  the behavior is pseudoplastic and, when  $n > 1$ , the fluid is dilatant.

The Ostwald-de-Waele power-law model represents several non-Newtonian fluids of practical interest and therefore has been used in this paper. Christopher and Middleman (1965) and Dharmadhikari and Kale (1985) proposed the following relationships for the permeability as a function of the power law index  $n$  as follows:

$$K = \begin{cases} \frac{6}{25} \left\{ \frac{n\varepsilon}{3n+1} \right\}^n \left\{ \frac{\varepsilon d}{3(1-\varepsilon)} \right\}^{n+1} & \text{(Christopher and Middleman)} \\ \frac{2}{\varepsilon} \left\{ \frac{d\varepsilon^2}{8(1-\varepsilon)} \right\}^{n+1} \left\{ \frac{6n+1}{10n-3} \right\} \left\{ \frac{16}{75} \right\}^{(3(10n-3)/(10n+11))} & \text{(Dharmadhikari and Kale),} \end{cases} \tag{6b}$$

where  $d$  is the particle diameter while  $\varepsilon$  is the porosity. When  $n < 1$  the model describes pseudoplastic behavior, whereas  $n > 1$  represents dilatant behavior.

We introduce the following dimensionless variables (see El-Amin (2003)):

$$t = \frac{U\bar{t}}{L}, \quad x = \frac{\bar{x}}{L}, \quad y = \frac{\bar{y}}{L}, \quad u = \frac{\bar{u}}{U}, \quad v = \frac{\bar{v}}{U}, \quad \theta = \frac{\bar{T} - \bar{T}_\infty}{\bar{T}_w - \bar{T}_\infty} \quad \text{and} \quad \phi = \frac{\bar{C} - \bar{C}_\infty}{\bar{C}_w - \bar{C}_\infty}, \tag{7}$$

where  $U = [\rho L^n / k]^{1/n-2}$  is the reference velocity and  $L$  is a suitable length scale.

Introducing expressions (7) into equations (1) - (4) we have the transformed equations in the following form:

$$\frac{\partial u}{\partial x} + \frac{\partial v}{\partial y} = 0 \tag{8}$$

$$\frac{\partial u}{\partial t} + u \frac{\partial u}{\partial x} + v \frac{\partial u}{\partial y} = Gr_\theta \theta + Gr_\phi \phi + \frac{\partial}{\partial y} \left( \left| \frac{\partial u}{\partial y} \right|^{n-1} \frac{\partial u}{\partial y} \right) - \frac{1}{Da} |u|^{n-1} u - \frac{Fr}{Da} |u| u \tag{9}$$

$$\frac{\partial \theta}{\partial t} + u \frac{\partial \theta}{\partial x} + v \frac{\partial \theta}{\partial y} = \frac{1}{Re} \left\{ \frac{1}{Pr} \frac{\partial^2 \theta}{\partial y^2} + D_f \frac{\partial^2 \phi}{\partial y^2} \right\} \tag{10}$$

$$\frac{\partial \phi}{\partial t} + u \frac{\partial \phi}{\partial x} + v \frac{\partial \phi}{\partial y} = \frac{1}{Re} \left\{ \frac{1}{Sc} \frac{\partial^2 \phi}{\partial y^2} + Sr \frac{\partial^2 \theta}{\partial y^2} \right\}, \tag{11}$$

where

$$Gr_\theta = \frac{Lg\beta(\bar{T}_w - \bar{T}_\infty)}{U^2} \text{ is the local temperature Grashof number,}$$

$$Gr_\phi = \frac{Lg\beta^*(\bar{C}_w - \bar{C}_\infty)}{U^2} \text{ is the local mass Grashof number,}$$

$$Da = \frac{K}{\varepsilon^n L^{n+1}} \text{ is the Darcy number and } Fr = \frac{FK^{1/2}}{\varepsilon^{n-2} L^n} \text{ is the inertia coefficient.}$$

$$D_f = \frac{\rho D_m k_T (\bar{C}_w - \bar{C}_\infty)}{\mu c_s c_p (\bar{T}_w - \bar{T}_\infty)} \text{ is the Dufour number, } Sc = \frac{\mu}{\rho D_m} \text{ is the Schmidt number,}$$

$$Sr = \frac{\rho D_m k_T (\bar{T}_w - \bar{T}_\infty)}{\mu T_m (\bar{C}_w - \bar{C}_\infty)} \text{ is the Soret number, } Pr = \frac{\mu c_p}{k_f} \text{ is the Prandtl number and}$$

$$Re = \frac{LU\rho}{\mu} \text{ is the Reynolds number.}$$

The initial and boundary conditions are now given by:

$$\begin{aligned} t = 0: & \quad u = v = \theta = \phi = 0 & \quad \text{for all } x \text{ and } y \\ t > 0: & \quad \begin{cases} u = v = \theta = \phi = 0 & \text{at } x = 0, \forall y \\ u = v = 0, \theta = \phi = 1 & \text{at } x > 0, y = 0 \\ u = 0, \theta \rightarrow 0, \phi \rightarrow 0 & \text{at } x > 0 \text{ as } y \rightarrow \infty \end{cases} \end{aligned} \quad (12)$$

In technological applications, the wall shear stress and the local Nusselt number are of primary interest.

The wall shear stress may be written as:

$$\tau_w = \mu \left( \frac{\partial u}{\partial y} \right)^n \Big|_{y=0} = \mu \frac{U^n}{L^n} \left( \frac{\partial u}{\partial y} \right)^n \Big|_{y=0} \quad (13)$$

Therefore, the local friction factor is given by

$$C_f = \frac{2\tau_w}{\rho U^2} = 2 \left( \frac{\partial u}{\partial y} \right)^n \Big|_{y=0} \quad (14)$$

From the definition of the local surface heat flux is defined by

$$q_w = -k_f \frac{\partial \bar{T}}{\partial y} \Big|_{y=0} = -\frac{k_f (\bar{T}_w - \bar{T}_\infty)}{L} \frac{\partial \theta}{\partial y} \Big|_{y=0}, \quad (15)$$

where,  $k_f$  is the thermal conductivity of the saturated porous medium, together with the definition of the local Nusselt number

$$Nu = \frac{q_w}{\bar{T}_w - \bar{T}_\infty} \frac{L}{k_f} = -\left. \frac{\partial \theta}{\partial y} \right|_{y=0} \quad (16)$$

Finally the local surface mass flux is defined by

$$Q_w = -D_m \left. \frac{\partial \bar{C}}{\partial y} \right|_{\bar{y}=0} = -\frac{D_m (\bar{C}_w - \bar{C}_\infty)}{L} \left. \frac{\partial \phi}{\partial y} \right|_{y=0} \quad (17)$$

Therefore, the local Sherwood number is given by

$$Sh = \frac{Q_w}{\bar{C}_w - \bar{C}_\infty} \frac{L}{D_m} = -\left. \frac{\partial \phi}{\partial y} \right|_{y=0} \quad (18)$$

### 3. Numerical Method

The numerical integrations were carried out on the time dependent form of the nonlinear partial differential equations (8) - (11), with initial and boundary conditions (12) by the explicit finite-difference method, as explained by Carnahan et al. (1969). The spatial domain under investigation was restricted to finite dimensions. Here, the length of the plate  $X_{max}$  was assumed to be 2.4 and the boundary layer thickness  $Y_{max}$  was taken as 1.28. The region to be examined in  $(x, y, t)$  space is covered by a rectilinear grid with sides parallel to axes with  $\Delta x, \Delta y, \Delta t$  the grid spacing in  $x, y$  and  $t$  directions respectively.

The grid point  $(x, y, t)$  are given by  $(i\Delta x, j\Delta y, m\Delta t)$  where the velocities, temperature and concentration fields were calculated for various time steps for a  $24 \times 30$  grid. The grid sizes are taken as  $\Delta x = 0.1, \Delta y = 0.008$  at  $j = 1(1)4$ ,  $\Delta y = 0.01$  at  $j = 5$ ,  $\Delta y = 0.014$  at  $j = 6$ ,  $\Delta y = 0.016$  at  $j = 7, 8$ ,  $\Delta y = 0.024$  at  $j = 9$ ,  $\Delta y = 0.048$  at  $j = 10$ ,  $\Delta y = 0.056$  at  $j = 11(1)30$  and  $\Delta t = 0.05$ . An examination of complete results for  $m=10, 20, 30, \dots, 130, 150$  or  $(t = 0.5, 1, 1.5, \dots, 6.5, 7.5)$  revealed little or no change in  $u, v, \theta$  and  $\phi$  after  $m = 100$  ( $t = 5$ ) for all computations. Thus the results for  $t = 6.5$  are essentially the steady-state values.

Notice that, the uniform scheme in  $x$  and  $t$  directions and non-uniform scheme in direction of  $y$  are used for solving this problem.

Consider  $u', v', \theta'$  and  $\phi'$  denote the values of  $u, v, \theta$  and  $\phi$  at the end of a time-step. Then, the approximate set of finite difference equations corresponding to equations. (8)-(11) are

$$\frac{(u'_{i,j} - u'_{i-1,j})}{\Delta x} + \frac{(v'_{i,j} - v'_{i,j-1})}{\Delta y} = 0 \quad (19)$$

$$\begin{aligned} \frac{(u'_{i,j} - u_{i,j})}{\Delta t} + u_{i,j} \frac{(u_{i,j} - u_{i-1,j})}{\Delta x} + v_{i,j} \frac{(u_{i,j+1} - u_{i,j})}{\Delta y} &= Gr_{\theta} \theta'_{i,j} + Gr_{\phi} \phi'_{i,j} \\ &+ \frac{\left( \left| \frac{(u_{i,j+1} - u_{i,j})}{\Delta y} \right|^{n-1} \frac{(u_{i,j+1} - u_{i,j})}{\Delta y} - \left| \frac{(u_{i,j} - u_{i,j-1})}{\Delta y} \right|^{n-1} \frac{(u_{i,j} - u_{i,j-1})}{\Delta y} \right)}{\Delta y} \end{aligned} \quad (20)$$

$$\begin{aligned} & - \frac{1}{Da} |u_{i,j}|^{n-1} u_{i,j} - \frac{Fr}{Da} |u_{i,j}| u_{i,j} \\ \frac{(\theta'_{i,j} - \theta_{i,j})}{\Delta t} + u_{i,j} \frac{(\theta_{i,j} - \theta_{i-1,j})}{\Delta x} + v_{i,j} \frac{(\theta_{i,j+1} - \theta_{i,j})}{\Delta y} & \\ = \frac{1}{Re} \left[ \frac{1}{Pr} \frac{(\theta_{i,j+1} - 2\theta_{i,j} + \theta_{i,j-1})}{(\Delta y)^2} + D_f \frac{(\phi_{i,j+1} - 2\phi_{i,j} + \phi_{i,j-1})}{(\Delta y)^2} \right] & \end{aligned} \quad (21)$$

$$\begin{aligned} \frac{(\phi'_{i,j} - \phi_{i,j})}{\Delta t} + u_{i,j} \frac{(\phi_{i,j} - \phi_{i-1,j})}{\Delta x} + v_{i,j} \frac{(\phi_{i,j+1} - \phi_{i,j})}{\Delta y} & \\ = \frac{1}{Re} \left[ \frac{1}{Sc} \frac{(\phi_{i,j+1} - 2\phi_{i,j} + \phi_{i,j-1})}{(\Delta y)^2} + Sr \frac{(\theta_{i,j+1} - 2\theta_{i,j} + \theta_{i,j-1})}{(\Delta y)^2} \right], & \end{aligned} \quad (22)$$

where, primed variables indicate the values of the variables at a new time and  $(i, j)$  represent grid points. The coefficients  $u_{i,j}$  and  $v_{i,j}$  in equations (20), (21) and (22) are treated as constants, during any one time-step. Then, at the end of any time-step  $\Delta t$ , the new velocity components  $u'$ ,  $v'$ , the new temperature  $\theta'$  and the new concentration  $\phi'$  at all interior grid points may be obtained by successive applications of (19) - (22), respectively. This process is repeated in time and provided the time-step is sufficiently small,  $u$ ,  $v$ ,  $\theta$  and  $\phi$  should eventually converge to values which approximate the steady state solution of equations (19) - (22).

$$\begin{aligned} t = 0 : & \quad u = v = \theta = \phi = 0 & \quad \text{for all } x \text{ and } y \\ t > 0 : & \begin{cases} u = v = \theta = \phi = 0 & \text{at } x = 0, \forall y \\ u = v = 0, \theta = \phi = 1 & \text{at } x > 0, y = 0 \\ u = 0, \theta \rightarrow 0, \phi \rightarrow 0 & \text{at } x > 0 \text{ as } y \rightarrow \infty \end{cases} \end{aligned} \quad (23)$$

#### 4. Results and Discussion

The numerical computations were done by the symbolic computation software MATHEMATICA 5.2<sup>TM</sup>. The command (NSolve) was used to solve the linear systems (19) – (22) with the boundary condition. Computations are carried out until the steady-state solution used have been reached when the absolute difference between the values of velocity and

temperature as well as concentration at two consecutive time steps is less than  $10^{-5}$  at all grid points.

Details of the velocities, temperature and concentration fields were presented in curves and tables 1, 2 for various values of the time and the parameters of the problem, e.g. the inertia coefficient  $Fr$  and the Reynolds number  $Re$ . Figure 2 to Figure 11 presented fully numerical results for the velocity and temperature profiles as well as the concentration distributions. A selection set of results have been obtained covering the ranges  $0 \leq Fr \leq 1000$ ,  $0.1 \leq Da \leq 1000$ ,  $-0.001 \leq Gr_\theta \leq 0.001$ ,  $-0.005 \leq Gr_\phi \leq 0.005$  and  $1 \leq Re \leq 10$  at  $Sr = 0.1$ ,  $Sc = 7$ ,  $D_f = 0.12$ ,  $Pr = 10$  and  $n = 2$  (the fluid is dilatant). Figure 2 - Figure 4 showed the transient profiles of velocity  $u$  and  $v$  and temperature  $\theta$  as a function of  $y$  for various values of  $t$ , respectively at  $Re = 1$ ,  $Fr = 10$ ,  $Da = 1$ ,  $Gr_\theta = 0.001$ ,  $Gr_\phi = 0.005$ ,  $Pr = 10$ ,  $Sr = 0.1$ ,  $Sc = 7$ ,  $D_f = 0.12$  and  $n = 2$ .

It can be seen from these figures that, after certain times the distribution of the velocities and temperature are affected by its position from  $y$ . However, the velocity  $-v$  grows as  $y$  increases from the origin point to the leading edge, while the opposite is true for the temperature. Also, the time enhances the velocities  $u$  and  $-v$  and temperature  $\theta$ , and after advancing time steps the effect of time on them tends to disappear. This means that unsteady-state tends to approach steady-state.

Steady velocity profiles  $u$  and  $-v$  as functions of  $y$  (plate length) for various values of the inertia coefficient  $Fr$  were illustrated in Figures 5 and 6, respectively at  $Re = 1$ ,  $Da = 1$ ,  $Gr_\theta = 0.001$ ,  $Gr_\phi = 0.005$ ,  $Pr = 10$ ,  $Sr = 0.1$ ,  $Sc = 7$ ,  $D_f = 0.12$ ,  $n = 2$  and  $t = 6.5$  (steady state). It is noteworthy that, the inertia coefficient  $Fr$  reduces the velocity  $v$  while it has a slight effect on the velocity  $u$  (large values of  $Fr$  have an essential effect on the velocities).

In Figures 7 - 10, the velocity profiles and the temperature profiles as well as the concentration distributions as functions of  $y$  for various values of  $Re$  (in the steady state) are plotted, respectively at  $Fr = 10$ ,  $Da = 1$ ,  $Gr_\theta = 0.001$ ,  $Gr_\phi = 0.005$ ,  $Pr = 10$ ,  $Sr = 0.1$ ,  $Sc = 7$ ,  $D_f = 0.12$  and  $n = 2$ . From these figures one can note that, all of these distributions decrease as  $Re$  increases. This is expected since the decreasing of the Reynolds number  $Re$  causes the thermal boundary layer to become thicker and the fluid to be warmer.

Figure 11 describes the behavior of the velocities, temperature and concentration distributions (in the steady state) in three dimension profiles at  $Re = 1$ ,  $Fr = 10$ ,  $Da = 1$ ,  $Gr_\theta = 0.001$ ,  $Gr_\phi = 0.005$ ,  $Pr = 10$ ,  $Sr = 0.1$ ,  $Sc = 7$ ,  $D_f = 0.12$  and  $n = 2$  (dilatant fluid).

Table 1 represents the variation of transient friction factor  $\frac{C_f}{2}$ , Nusselt number  $Nu$  and Sherwood number  $Sh$  for dilatant fluid ( $n > 1$ ) with various values of the time and inertia coefficient  $Fr$  at  $Re = 1$ ,  $Da = 10$ ,  $Gr_\theta = 0.0002$ ,  $Gr_\phi = 0.001$ ,  $Pr = 10$ ,  $Sr = 0.1$ ,  $Sc = 7$ ,  $D_f = 0.12$  and  $n = 2$ . It can be seen that the friction factor increases as time increases until approach

steady state, while the heat transfer rate in terms of Nusselt number and the mass transfer rate in terms of Sherwood number are reduced with increasing of time.

Also, from this table, it can be seen that due to an increase in  $Fr$  there is a fall in the Nusselt number and the Sherwood number, while due to an increase in inertia coefficient  $Fr$  there is an increase in the wall shear stress. Finally, in table 2 the friction factor, the Nusselt number and the Sherwood number values are presented for different values of the Darcy number  $Da$ , the local temperature Grashof number  $Gr_\theta$  and the local mass Grashof number  $Gr_\phi$ , respectively at  $Re=1$ ,  $Fr = 10$ ,  $Pr = 10$ ,  $Sr = 0.1$ ,  $Sc = 7$ ,  $D_f = 0.12$ ,  $n = 2$  (for dilatant fluid),  $t = 1.5$  (in the unsteady state) and  $x = 0.1$ . The friction factor, the heat transfer rate in terms of Nusselt number and the mass transfer rate in terms of Sherwood number increase as  $Da$  increases.

The effect of the Darcy number  $Da$  becomes smaller as  $Da$  increases. Physically, this result can be achieved when the holes of the porous medium are very large so that the resistance of the medium can be neglected. On the other hand, the local temperature Grashof number  $Gr_\theta$  represents the effects of free convection currents. Since the free convection currents are in existence,  $(\bar{T}_w - \bar{T}_\infty)$  may be positive, zero or negative. Hence, the free convection parameter

(Grashoff number)  $Gr_\theta = \frac{Lg\beta(\bar{T}_w - \bar{T}_\infty)}{U^2}$  assumes positive, zero or negative values. Physically,

$Gr_\theta > 0$  corresponds to heating of the fluid (or cooling of the surface),  $Gr_\theta < 0$  corresponds to cooling of the fluid (or heating of the surface) and  $Gr_\theta = 0$  corresponds to the absence of the free convection currents. From this table one can note that, the local friction factor in equation (14) is negative in the fluid cooling case ( $Gr_\theta = -0.001, -0.0005$  and  $-0.0002$ ). Physically, this is possible because the flow of the fluid moving in the upward direction is now being opposed by the free convection currents and hence the velocity decreases. Thus, the flow of the fluid is of reverse type in the fluid cooling case.

Also from this table, it can be seen that due to an increase in the local temperature Grashof number  $Gr_\theta$  and the local mass Grashof number  $Gr_\phi$ , there is an increase in the friction factor, the Nusselt number and the Sherwood number.

## 6. Conclusions

The finite difference method was used in this paper to compute unsteady natural convection with heat and mass transfer from an isothermal vertical flat plate to a non-Newtonian fluid saturated porous medium, which was modeled as a power-law fluid. Boundary layer and Boussinesq approximations had been introduced together with the Darcy-Brinkman-Forchheimer model to describe the flow field. Numerical calculations were carried out for the various parameters entering into the problem. Velocity, temperature and concentration profiles were shown graphically and the physical quantities of the problem were given in tables. It was found that as time approaches infinity, the values of friction factor, heat transfer and mass transfer coefficients approach the steady state values.

**Table 1:** Transient friction factor  $\frac{C_f}{2}$ , Nusselt number  $Nu$  and Sherwood number  $Sh$  for various values of  $t$  and  $Fr$  when  $Pr = 10, Sr = 0.1, Sc = 7, D_f = 0.12, n = 2,$   
 $Gr_\theta = 0.0002, Gr_\phi = 0.001$  and  $Da = 10$  at  $x = 0.1$ .

$t$	$C_f / 2 \times 10^4$			$Nu$			$Sh$		
	Fr=0.0	Fr=100	Fr=1000	Fr=0.0	Fr=100	Fr=1000	Fr=0.0	Fr=100	Fr=1000
0.5	0.1329	0.6535	0.7114	13.7637	13.7225	13.3940	13.7679	13.7661	13.7493
2.0	0.9561	0.9562	0.9565	12.6107	12.6106	12.6103	12.8335	12.8334	12.8331
4.0	1.2447	1.2448	1.2449	11.3076	11.3073	11.3051	11.7092	11.7090	11.7071
5.0	1.2955	1.2956	1.2957	10.6321	10.6320	10.6317	11.6256	11.6253	11.6223
6.0	1.3890	1.3895	1.3930	10.4545	10.4544	10.4535	10.9973	10.9972	10.9964
6.5	9.7805	10.308	17.222	9.5680	9.5665	9.5513	10.5581	10.5579	10.5566
$\infty$	9.7805	10.308	17.222	9.5680	9.5665	9.5513	10.5581	10.5579	10.5566

**Table 2:** The friction factor  $\frac{C_f}{2}$ , Nusselt number  $Nu$  and Sherwood number  $Sh$  for different values of  $Da, Gr_\theta$  and  $Gr_\phi$  when  $Sr = 0.1, Sc = 7, D_f = 0.12, Re = 1, n = 2, Fr = 10, Pr = 10$  and  $t = 1.5$  at  $x = 0.1$ .

$Da$	$Gr_\theta$	$Gr_\phi$	$C_f / 2 \times 10^4$	$Nu$	$Sh$
0.1	0.0002	0.001	0.83401935300	12.98447391869	13.15162736906
1.0			0.83403652798	12.98447392039	13.15162737051
10			0.83403824551	12.98447392056	13.15162737066
100			0.83403841726	12.98447392058	13.15162737068
1000			0.83403843444	12.98447392058	13.15162737068
1.0	-0.001	0.001	-0.0068725020	12.98439789733	13.15156205198
	-0.0005		-0.0009604872	12.98444326492	13.15160102994
	-0.0002		-0.00001445515	12.98445837635	13.15161401429
	0.0		0.74928377348	12.98446659597	13.15162107699
	0.0002		0.83401935300	12.98447391869	13.15162736906
	0.001		1.10997579050	12.98449795091	13.15164801892
1.0	0.0002	-0.001	-0.65376079951	12.98435584981	13.15152592396
		0.0	0.34942311552	12.98443267696	13.15159193248
		0.001	0.83403652798	12.98447392039	13.15162737051
		0.005	1.20002650210	12.98455425091	13.15169639448

## REFERENCES

- Anwar Hossain, M. and Wilson, M. (2002). Natural Convection Flow in a Fluid Saturated Porous Medium Enclosed by Non-Isothermal Walls with Heat Generation, *International Journal of Thermal Sciences*, Vol. 41, pp. 447-454.
- Carnahan, B., Luther, H. A. and Wilkes, J. O. (1969). *Applied numerical methods*, John Wiley, New York.
- Christopher, R. H. and Middleman, S. (1965). Power-Law Flow through a Packed Tube, *I & EC Fundamentals*, Vol. 4, pp. 422-426.
- Dharmadhikari, R. V. and Kale, D. D. (1985). Flow of Non-Newtonian Fluids through Porous Media, *Chemical Eng. Sci.*, Vol. 40, pp. 527-529.
- El-Amin, M. F. (2003). Combined Effect of Magnetic Field and Viscous Dissipation on a Power-Law Fluid over Plate with Variable Surface Heat Flux Embedded in a Porous Medium, *Journal of Magnetism & Magnetic Materials*, Vol. 261, pp. 228-237.
- Hady, F. M. and Ibrahim, F. S. (1997). Forced Convection Heat Transfer on a Flat Plate Embedded in Porous Media for Power-Law Fluids, *Transport in porous media*, Vol. 28, pp. 125-134.
- Inoue, M. and Nakayama, A. (1998) Numerical Modeling of Non-Newtonian Fluid Flow in a Porous Medium Using a Three Dimensional Periodic Array, *Transactions of the ASME, Journal of Fluid Eng.*, Vol. 120, 1, pp. 131-135.
- Israel-Cookey, C., Ogulu, A. and Omubo-Pepple, V. B. (2003). Influence of Viscous Dissipation and Radiation on Unsteady MHD Free-Convection Flow past an Infinite Heated Vertical Plate in a Porous Medium with Time-Dependent Suction, *International Journal of Heat and Mass Transfer*, Vol. 46, pp. 2305-2311.
- Kinyanjui, M., Wanza, J. K. K and Uppal, S. M. (2001). Magnetohydrodynamic Free Convection Heat and Mass Transfer of a Heat Generating Fluid past an Impulsively Started Infinite Vertical Porous Plate with Hall Current and Radiation Absorption, *Energy Conversion and Management*, Vol. 42, pp. 917-931.
- Kok Siong Chiem and Yong Zhao (2004). Numerical Study of Steady/Unsteady Flow and Heat Transfer in Porous Media Using a Characteristics-Based Matrix-Free Implicit FV Method on Unstructured Grids, *International Journal of Heat and Fluid Flow*, Vol. 25, pp. 1015-1033.
- Pascal, H. (1992). Similarity Solutions to Some Unsteady Flows of Non-Newtonian Fluids of Power Law Behavior, *International Journal of Non-Linear Mechanics*, Vol. 27, pp. 759-771.
- Pascal, J. P. (1992). Similarity Solutions for Axisymmetric Plane Radial Power Law Fluid Flows through a Porous Medium, *Computers & Mathematics with Applications*, Vol. 23, pp. 25-41.
- Pascal, J. P. and Pascal, H. (1997). Non-Linear Effects on Some Unsteady Non-Darcian Flows through Porous Media, *International Journal of Non-Linear Mechanics*, Vol. 32, pp. 361-376.
- Shenoy, A. V. (1993). Darcy-Forchheimer Natural, Forced and Mixed Convection Heat Transfer in Non-Newtonian Power-Law Fluid Saturated Porous Media, *Transport in Porous Media*, Vol. 11, pp. 219-241.
- Shulman, Z. P., Baykov, B. I. and Zaltsgendler, E. A. (1975). *Heat and mass transfer in free convection of non-Newtonian fluids*, Naukai tehnika, Minsk (in Russian).
- Shvets, Yu. I. and Vishevskiy, V. K. (1987). Effect of Dissipation on Convective Heat Transfer in Flow of Non-Newtonian Fluids, *Heat Transfer-Soviet Res.*, Vol. 19, pp. 38-43.

Wen T. Cheng and Hsiao T. Lin (2002). Unsteady Forced Convection Heat Transfer on a Flat Plate Embedded in the Fluid-Saturated Porous Medium with Inertia Effect and Thermal Dispersion, International Journal of Heat and Mass Transfer, Vol. 45, pp. 1563-1569.

### Nomenclature

$C_f$	friction factor	$F$	empirical constant
$C_p$	specific heat	$N$	power-law index
$D$	pore diameter	$Gr_\theta$	local temperature Grashof number
$g$	acceleration due to gravity	$Gr_\phi$	local mass Grashof number
$K$	Permeability	<b>Symbols</b>	
$k$	non-Newtonian consistency index	$\theta$	dimensionless temperature
$k_f$	thermal conductivity of fluid	$\phi$	dimensionless concentration
$q_w, Q_w$	heat transfer coefficient and mass transfer coefficient	$\tau_w$	wall shear stress
$\bar{t}$	time	$\tau_{ij}$	stress tensor component
$T$	dimensionless time	$e_{ij}$	strain rate tensor component
$\bar{T}$	Temperature	$\beta$	coefficient of thermal expansion
$\bar{C}$	Concentration	$\beta^*$	coefficient of expansion with concentration
$\bar{u}, \bar{v}$	dimensionless velocity components	$\mu$	dynamic viscosity
$u, v$	velocity components	$\rho$	density of the fluid
$\bar{x}, \bar{y}$	space coordinates	$\varepsilon$	porosity
$x, y$	dimensionless space coordinates	<b>Subscripts</b>	
$Nu$	Nusselt number	$w$	wall
$Sh$	Sherwood number	$\infty$	infinity
$Pr$	Prandtl number		

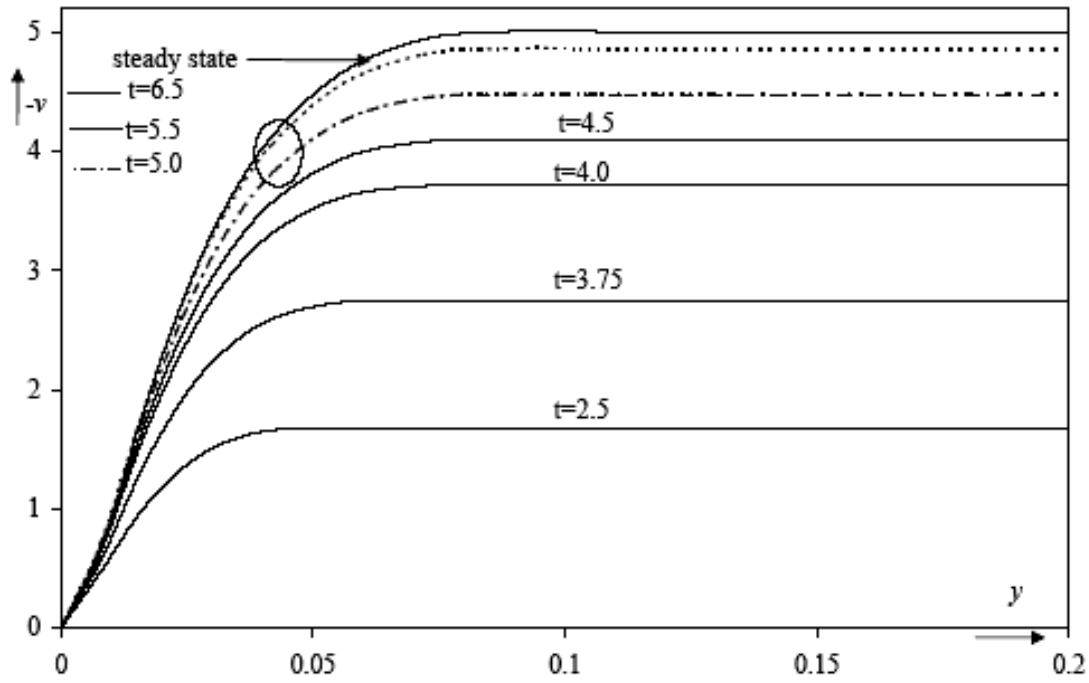


Figure 2. Transient velocity profiles  $-v$  as a function of  $y$  for various of  $t$ .

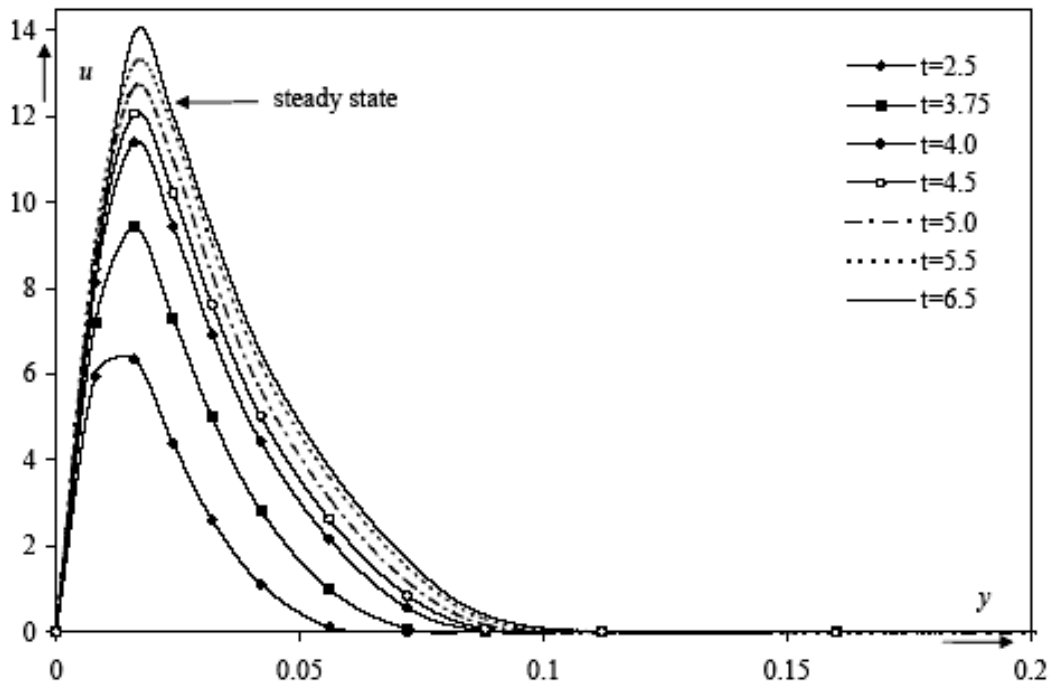


Figure 3. Transient velocity profiles  $u$  as a function of  $y$  for various of  $t$ .

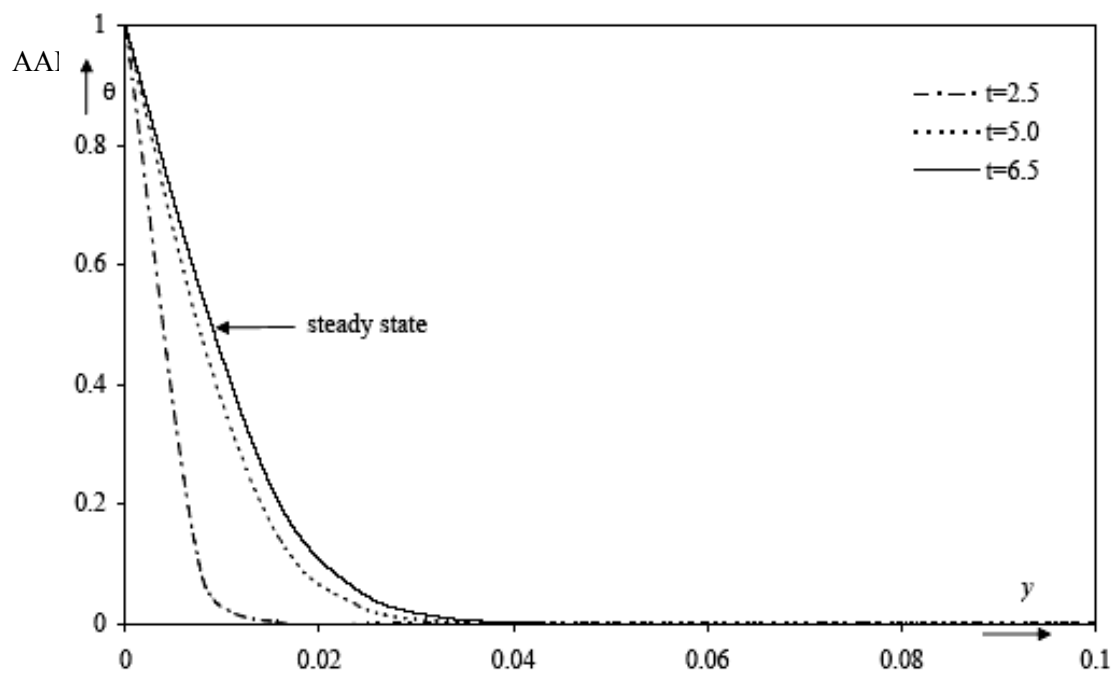


Figure 4. Transient temperature profiles as a function of  $y$  for various of  $t$ .

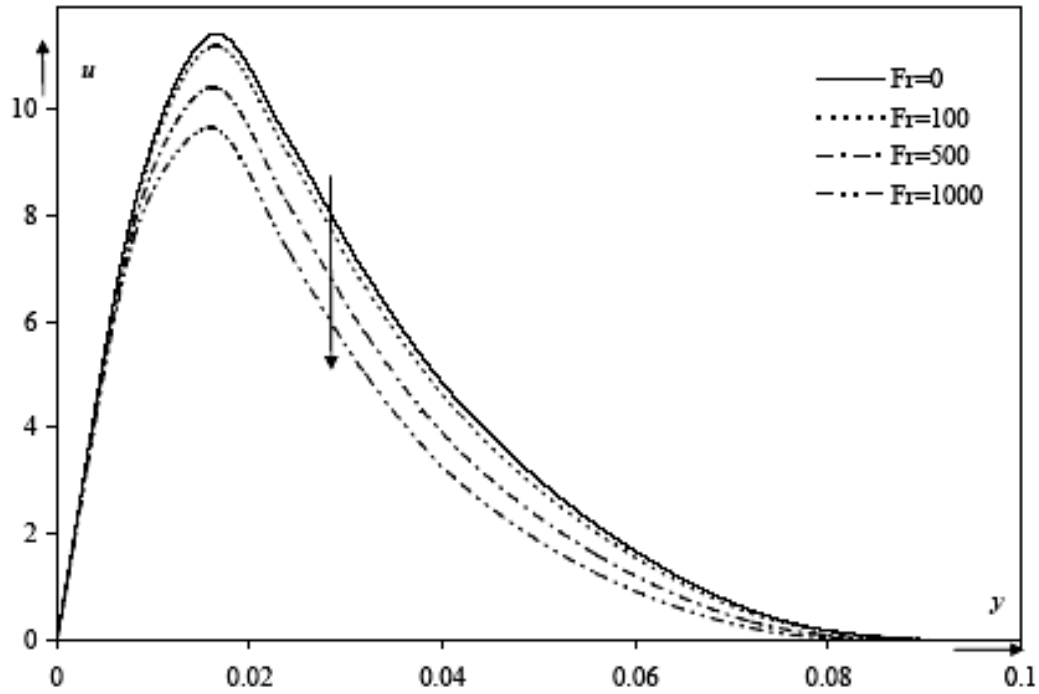


Figure 5. Velocity profiles  $u$  as a function of  $y$  for various of  $Fr$ .

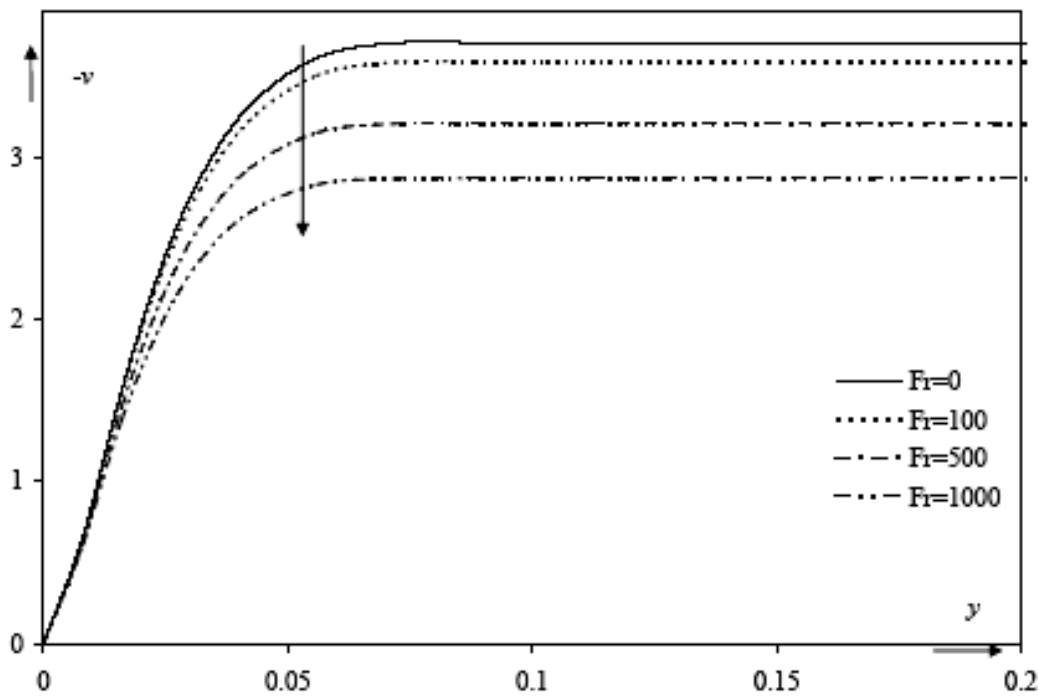


Figure 6. Velocity profiles  $-v$  as a function of  $y$  for various of  $Fr$ .

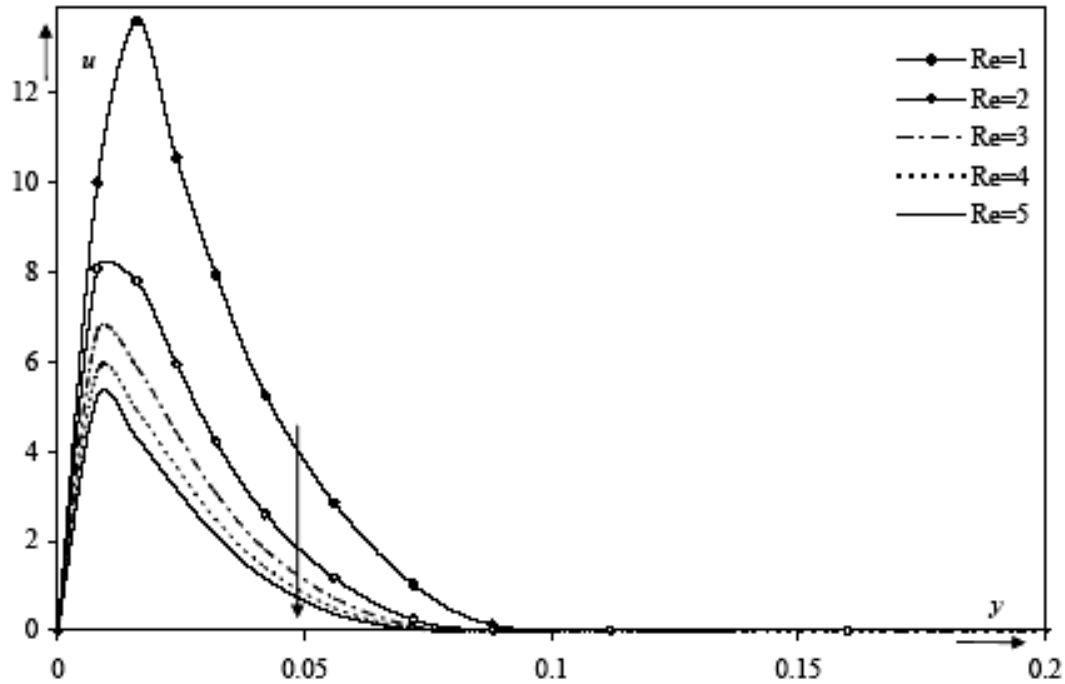


Figure 7. Velocity profiles  $u$  as a function of  $y$  for various of  $Re$ .

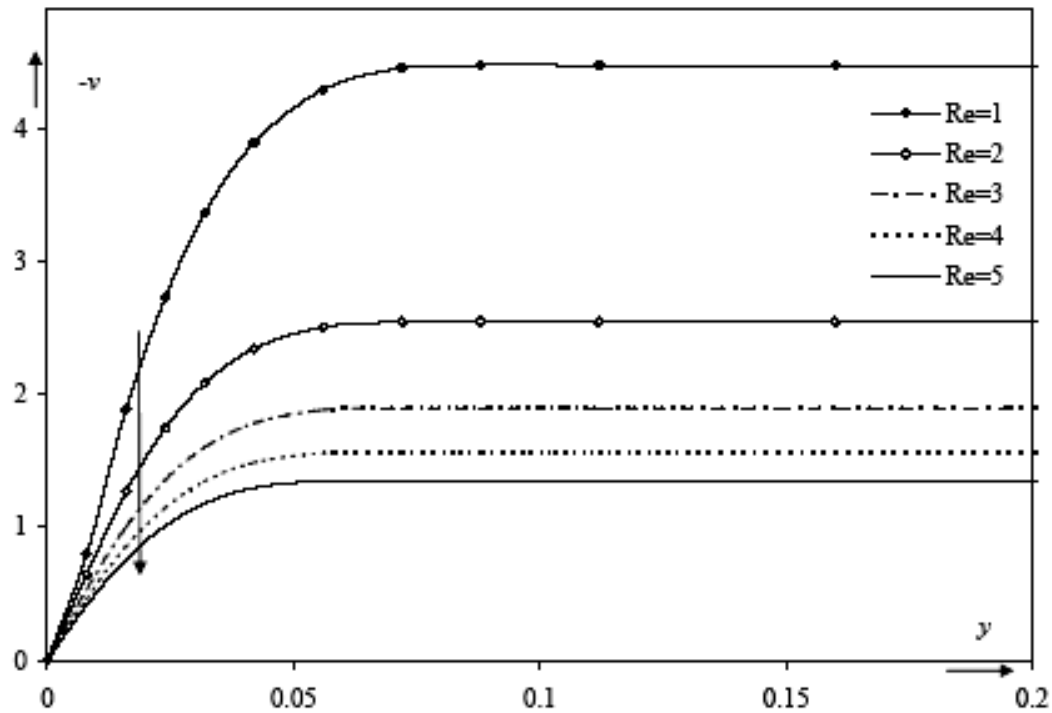
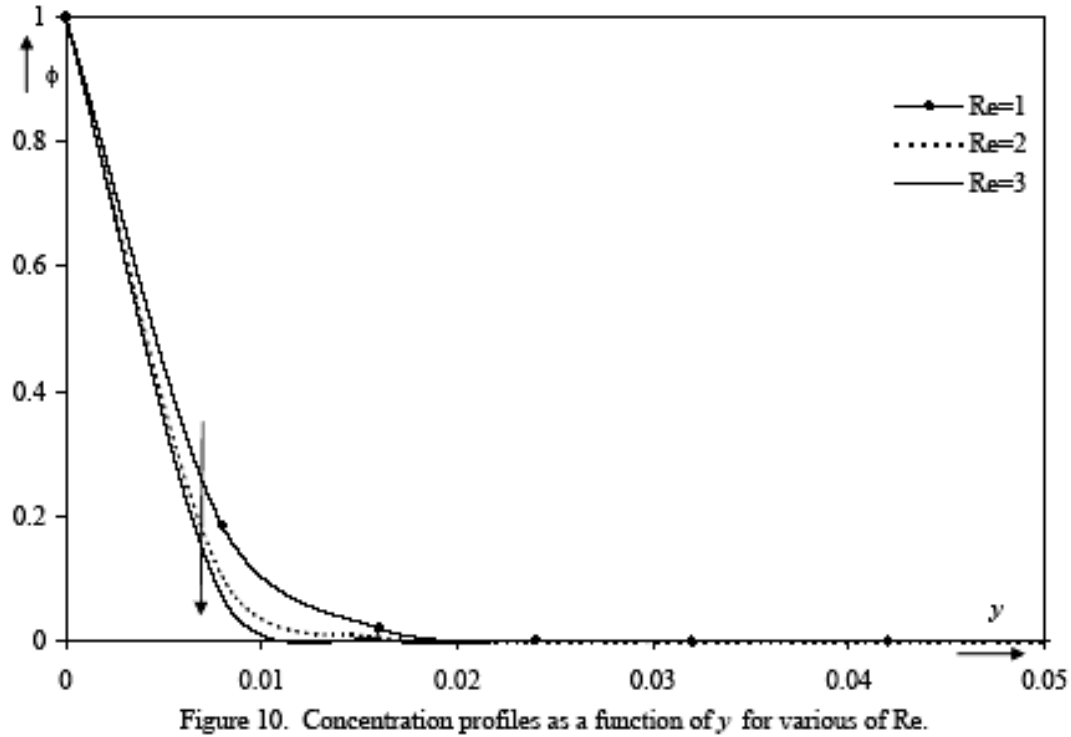
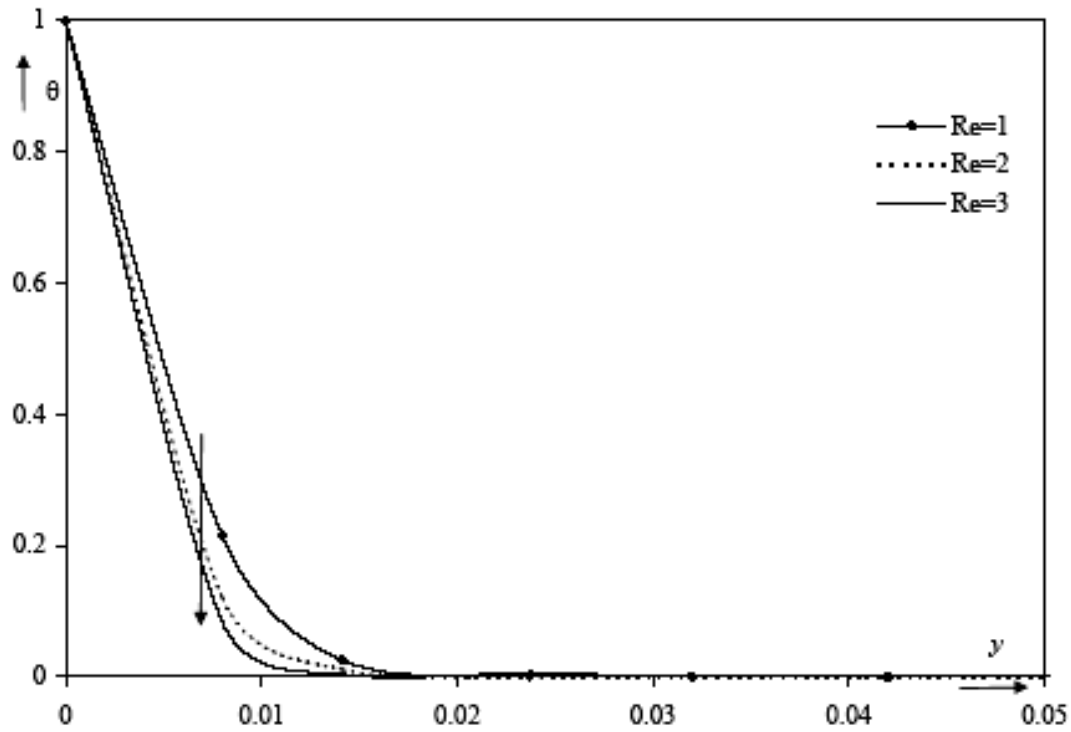


Figure 8. Velocity profiles  $-v$  as a function of  $y$  for various of  $Re$ .



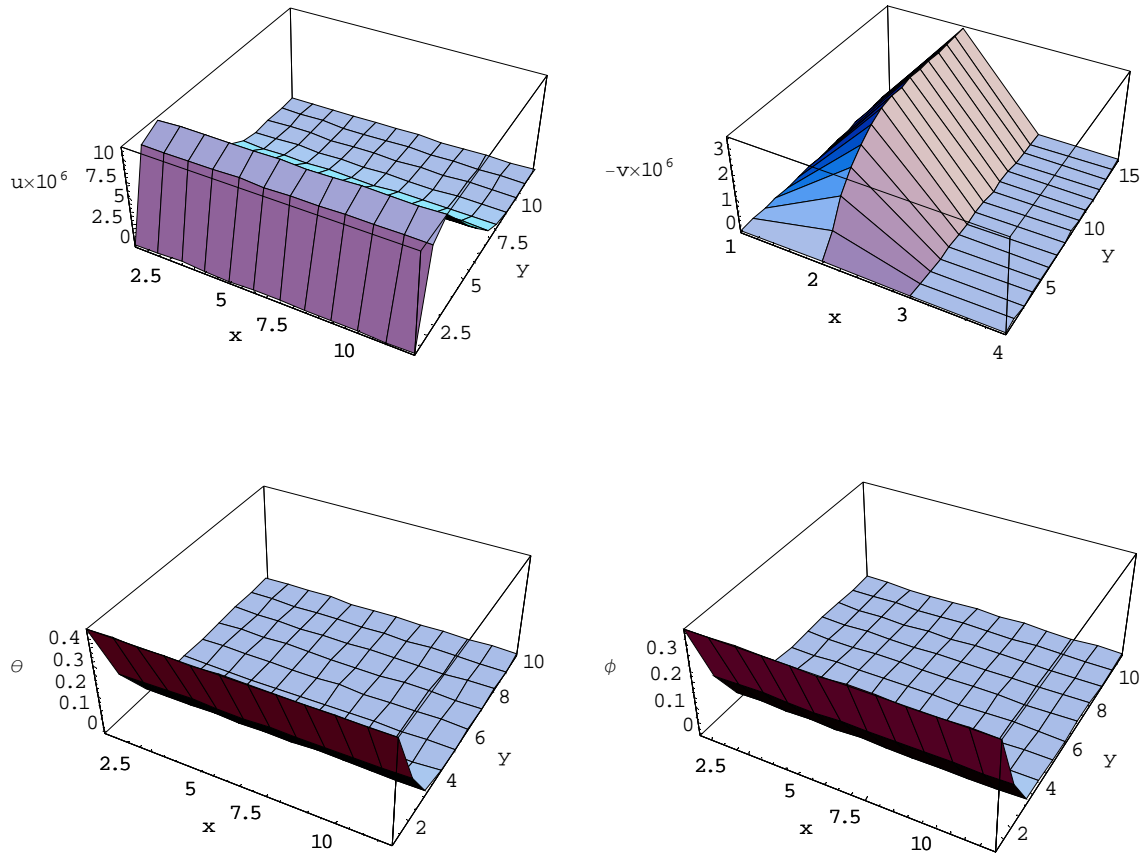


Figure 11. The velocities, temperature and concentration distributions.